Construction and Building Materials 115 (2016) 304–318

Contents lists available at ScienceDirect

Construction and Building Materials

journal homepage: www.elsevier.com/locate/conbuildmat

Prediction of strength and drift capacity of corroded reinforced concrete columns

Ngoc Son Vu [a], Bo Yu [b], Bing Li [a,*]

[a] School of Civil and Environmental Engineering, Nanyang Technological University, Singapore 639798
[b] Key Laboratory of Disaster Prevention and Structural Safety of Ministry of Education of China, School of Civil Engineering & Architecture, Guangxi University, Nanning 530004, China

HIGHLIGHTS

- A 3D non-linear finite element model for corroded RC columns was developed.
- The effects of key parameters on lateral load resistance and ultimate drift ratio of corroded RC columns was investigated.
- Prediction equations for lateral load resistance and ultimate drift ratio capacity of corroded RC columns were proposed.

ARTICLE INFO

Article history:
Received 3 December 2015
Received in revised form 6 March 2016
Accepted 10 April 2016
Available online 22 April 2016

Keywords:
Reinforced concrete column
Corroded reinforcement
Corrosion level
Finite element analysis
Lateral load resistance
Ultimate drift capacity

ABSTRACT

Steel reinforcement corrosion has been recognized as a major deterioration issue for the performance and safety of reinforced concrete (RC) structures. In this paper, the behavior of corroded RC columns under the seismic loading was studied using a three-dimensional (3D) non-linear Finite Element (FE) analysis, considering the material properties deterioration of reinforcement and concrete induced by corrosion. The experimental results of nine reinforced concrete (RC) columns in three experimental studies in literature were selected to verify the accuracy of the proposed 3D non-linear FE model. Thereafter, an extensive parametric investigation, including the FE models of 240 RC columns subjected to the simulated seismic loading was performed to study the influence of various crucial parameters on the seismic performance of corroded RC columns, particularly their lateral load resistance and ultimate drift capacity deterioration. Finally, these key parameters were incorporated into two prediction equations of the lateral load resistance and ultimate drift capacity for corroded RC columns.

1. Introduction

Steel reinforcement corrosion has been considered as a main cause of deterioration for reinforced concrete (RC) structures in the corrosive environments. At the material level, the tensile stresses will develop at the interface between reinforcing bars and concrete because of the volumetric expansion of corrosion product induced by reinforcement corrosion, causing the cover concrete of RC structures to crack and eventually spall off as well as reducing the bond strength of reinforcement at these interfacial regions. In addition, the confinement effect of core concrete will be also decreased due to corrosion of transverse reinforcement, particularly its maximum compressive strength and ultimate strain [1]. With regard to the corroded reinforcement, some experimental studies in literature revealed that the cross-sectional area, strength and ultimate strain of steel reinforcement are significantly decreased due to corrosion [2–4]. As a result, these mechanical properties deteriorations of reinforcement and concrete adversely affect the long-term performance and safety of RC structures, especially these structures under severely corrosive environments and subjected to the seismic loading.

Previous research mainly focuses on the causes and mechanism of reinforcement corrosion and its influences on the deteriorations of reinforcement and concrete [5–8]. On the other hand, the corrosion effect on the performance of RC structures subjected to the seismic loading has relatively little concern. Recently, several experimental investigations on the seismic behavior of corroded RC columns have been carried out in literature [9–13], which revealed that the corrosion phenomenon strongly affects the global performance of these structures, particularly their strength and ultimate drift capacity. For instance, in the experimental program carried out by Meda et al. [13], comparing to the uncorroded column with the same specifications and loading conditions, the corroded column with the corrosion level of approximately 20%

* Corresponding author.
E-mail address: cbli@ntu.edu.sg (B. Li).

http://dx.doi.org/10.1016/j.conbuildmat.2016.04.048
0950-0618/

Notation

a	shear span defined as distance from maximum moment section to point of inflection
A_g	gross cross-sectional area of the RC column
A_{pit}	cross-sectional area of corroded reinforcement at the pitting location
$A_s(X_{corr})$	average corroded cross-sectional area of reinforcement
A_{stnom}	original cross-sectional area of reinforcement
A_v	cross-sectional area of transverse reinforcement
b_0	circumference of the RC column section
c_c	smaller of concrete cover and one-half spacing between reinforcing bars
D_0	diameter of uncorroded reinforcement
D_c	diameter of corroded reinforcement
DR_{ultC}	ultimate drift ratio capacity of corroded RC column
d	effective depth of RC column section
d_b	diameter of reinforcing bar
E_{force}	normalized hysteretic force error
E_{energy}	normalized hysteretic energy error
f'_c	compressive strength of concrete
f'_{cC}	compressive strength of corroded cover concrete
f'_t	tensile strength of uncorroded concrete
f'_{tC}	tensile strength of corroded concrete
f_{yh}	yield strength of stirrup
F_{cal}	calculated lateral force at corresponding displacements
F_{mea}	measured lateral force at corresponding displacements
F_i	lateral force corresponding to the i^{th} step
k	coefficient regarding to the diameter and roughness of reinforcement
K	confined strength coefficient
N	axial compression force
R	factor that predicts the change of bond strength due to the corroded reinforcement
s	bond slip
s_1, s_2, s_3	value of slip related to various bond conditions
S	spacing between stirrups
T_{corr}	corrosion initiation time
t	corrosion time
X_{corr}	corrosion level in terms of mass loss (%)
x	depth of corrosion attack
V_{nC}	lateral load resistance of corroded RC column
W_0	reinforcement weight before corrosion
W_1	corroded reinforcement weight after corrosion
w/c	water to cement ratio
w_{cr}	crack width due to corrosion penetration
Δ_i	lateral displacement corresponding to the i^{th} step
Ω_{mea}	measured area within the hysteresis loops
Ω_{cal}	calculated area within the hysteresis loops
α	yield and ultimate strength factor of reinforcement induced by pitting corrosion
β	ultimate strain factor of reinforcement induced by pitting corrosion
ε_1	average tensile strain in cracked concrete
ε_{co}	concrete strain at maximum concrete stress
ε_{cu}	ultimate strain of confined concrete
ε_{uo}	ultimate strain of uncorroded reinforcement
ε_{uc}	ultimate strain of corroded reinforcement
τ_{fC}	bond stress of corroded reinforcement
τ_{f0}	bond stress of uncorroded reinforcement
$\tau_{\max C}$	maximum bond stress of corroded reinforcement
$\tau_{\max 0}$	maximum bond stress of uncorroded reinforcement
υ_{cr}	ratio of the volumetric expansion of the corroded steel to the virgin steel
ρ_v	volumetric transverse reinforcement ratio

showed a decrease of 30% of the lateral load and 50% of the maximum displacement. Similarly, the experimental study conducted by Ma et al. [11] also indicated that the reduction of 50% ultimate displacement capacity and 20% of yield as well as ultimate forces can be found in the corroded RC column subjected to the corrosion level of 15% when comparing to the uncorroded column. Therefore, it is vital to quantify the corrosion effect and its interaction among the other important factors on the lateral load resistance and ductility deterioration of corroded RC columns, specifically column aspect ratio, axial force ratio, concrete strength, and reinforcement ratio.

This study aims to develop a 3D non-linear FE analysis to study the seismic performance of corroded RC columns that deliberates the influences of corrosion level and various key parameters. The effects of corrosion damage on RC columns can be modeled by adapting the material properties of corroded reinforcement, unconfined cover and confined core concrete, modifying the bond behavior between corroded reinforcement and concrete. The experimental results reported in literature are employed to validate the accuracy of the proposed 3D non-linear FE model. Thereafter, this proposed FE model is adopted to study the behavior of corroded RC columns in an extensive parametric investigation. Finally, based on the multivariable regression analysis, two prediction equations of the lateral load resistance and ultimate drift capacity are developed for corroded RC columns.

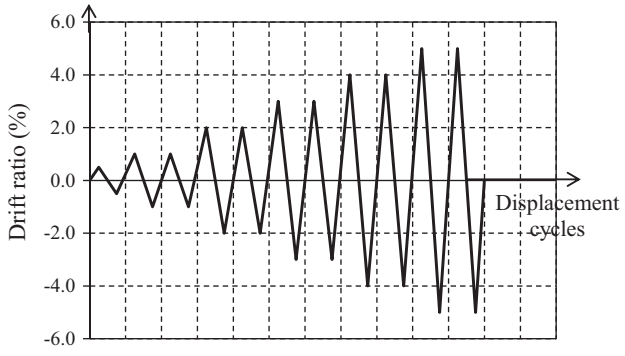

Fig. 1. Quasi-static cyclic loading history for FE model columns.

2. 3D non-linear finite element model of corroded RC column

2.1. General

In this paper, a 3D non-linear FE analysis was carried out to simulate the seismic behavior of RC columns with corroded reinforcement using DIANA [14] – a commercial non-linear FE software package. The validity and reliability of this FE software to model the behavior of corroded RC structures have been confirmed in literature [15–17].

In this proposed 3D non-linear FE model, concrete is modeled by adopting the twenty-node isoparametric solid brick element while the separate truss element which is connected to the concrete element using interface element is utilized to model the reinforcement. The local bond stress-slip law proposed in the CEB-FIP [18] is employed and modified to incorporate the corrosion effect in this study. A combination of a horizontal cyclic displacement and a vertical axial force is applied to simulate the

seismic loading on the corroded RC columns. The loading history is controlled by the drift ratio (DR) as shown in Fig. 1.

2.2. Modeling of unconfined cover concrete

Corrosion transforms steel into rust, resulting in the volumetric expansion that can develop the splitting stresses in concrete. The cracking and spalling of concrete induced by these stresses can be modeled by reducing the strength of concrete elements belonging to this region, as follows [19]:

$$f'_{cC} = \frac{f'_c}{1 + k\frac{\varepsilon_1}{\varepsilon_{co}}} \tag{1}$$

where k is the coefficient with regard to the diameter and roughness of reinforcement, the value $k = 0.1$ proposed in [20] is adopted in this study; ε_1 is the smeared tensile strain, regarding to the crack width of concrete due to corrosion, which can be estimated as:

$$\varepsilon_1 = \frac{\sum w_{cr}}{b_0} = \frac{\sum 2\pi(v_{cr} - 1)x}{b_0} \tag{2}$$

$$x = \frac{D_0 - D_c}{2} \tag{3}$$

where b_0 is the circumference of a RC column section; w_{cr} is the crack width induced by corrosion of reinforcement; x is the depth of corrosion attack; v_{cr} is the ratio of the volumetric expansion of the corroded steel to the virgin steel that depends on the type of corrosion products. The value of $v_{cr} = 2$ recommended by Molina et al. [21] is commonly employed in analytical studies of RC structures under corrosion of reinforcement [1,15,19].

According to the recommendation of Hanjari et al. [17], because of the cracked concrete around corroded reinforcement induced by corrosion, the tensile concrete strength should be reduced proportionally to the reduction in compressive concrete strength as following expression:

$$f'_{tC} = \frac{f'_{cC}}{f'_c} f'_t \tag{4}$$

where the tensile strength f'_t of uncorroded concrete estimated based on the CEB-FIP [18] as follows:

$$f'_t = 0.30(f'_c)^{2/3} \tag{5}$$

Fig. 2(a) and (b) present the modeling of cover concrete under compression and tension.

2.3. Modeling of corroded reinforcement

Generally, the average cross-sectional area of corroded reinforcement can be estimated as:

$$A_s(X_{corr}) = \frac{\pi D_0^2}{4}\left(1 - \frac{X_{corr}}{100}\right) \tag{6}$$

$$X_{corr} = \frac{W_0 - W_1}{W_0} * 100 \tag{7}$$

where $X_{corr}(\%)$ is the corrosion level which can be estimated based on the experimental measurement of the mass loss. When the experimental measurement is unavailable, the corrosion level can be predicted as following equations [22]:

$$X_{corr} = \frac{D_o^2 - D_c^2}{D_o^2} * 100 \tag{8}$$

$$D_c = D_0 - \frac{1.0508(1 - w/c)^{-1.64}}{d_c}(t - T_{corr})^{0.71} \tag{9}$$

where D_0, D_c are the diameters of the uncorroded and corroded reinforcing bars, respectively; T_{corr} is the starting time of corrosion; and t is the time after corrosion starts, more details can be found in [22].

In general, reinforcement corrosion in reinforced concrete structures is usually classified into two types: uniform corrosion caused by carbonation attack and pitting corrosion induced by the chloride penetration. Previous experimental studies in literature revealed that the stress-strain relationships of reinforcement are not seriously influenced by uniform corrosion [3,23]. Therefore, the mechanical properties of the corroded reinforcement induced by uniform corrosion can be simply modeled by reducing the cross-sectional area of uncorroded reinforcement as following Eq. (6). However, the yield and ultimate strengths of reinforcement due to pitting corrosion significantly deteriorate because of the stress concentration at the pitting location that can be estimated as follows [2]:

$$f = \left(1 - \alpha\frac{A_{pit}}{A_{stnom}}\right) f_o \tag{10}$$

where A_{stnom} is the original cross-sectional area of uncorroded reinforcement; A_{pit} is the residual cross-sectional area of corroded reinforcement at the pitting location and its calculation can be found in [2]. The value of the empirical coefficient $\alpha = 0.005$ suggested by Du et al. [3] is utilized in this paper.

Due to stress concentration at the pitting location, the ductility of corroded reinforcement reduces more drastically than its strength. In this study, the empirical equation developed by Du et al. [4] to calculate the ultimate strain of corroded reinforcement is adopted:

$$\varepsilon_{uc} = (1 - \beta X_{corr})\varepsilon_{u0} \tag{11}$$

where β is the empirical coefficient; $\beta = 0.03$ and $\beta = 0.05$ for a bare bar and a bar embedded in concrete, respectively. Fig. 2(d) indicates an example of modeling of stress-strain relationships for uncorroded and corroded reinforcing bars.

In this paper, the buckling of steel reinforcement in corroded RC columns under cyclic loading was modeled by adopting the stress-strain relationship of corroded reinforcement and the Monti-Nuti plasticity model [24] suggested in DIANA [14].

2.4. Modeling of confined concrete

As mentioned above, the corrosion of confinement reinforcement results in the properties degradation of confined core concrete, particularly the maximum strength and the ultimate strain which can be estimated when the transverse confining reinforcement fractures. In this paper, the stress-strain relationship developed by Mander et al. [25] is utilized and modified to simulate the behavior of confined concrete due to corrosion. According to this model, the confined strength and ultimate strain of concrete are estimated as:

$$f'_{cc} = Kf'_{co} \tag{12}$$

$$\varepsilon_{cu} = 0.004 + \frac{1.4\rho_s f_{yh}\varepsilon_{uc}}{f'_{cc}} \tag{13}$$

where f'_{cc}, f'_{co} are the confined and unconfined concrete strengths, respectively and K is the confined strength coefficient which depends on lateral confining stresses f'_{lx} and f'_{ly}, for details see [25]. To take into consideration the corrosion effect, this coefficient can be calculated by reducing the average cross-sectional area and strength of both longitudinal and transverse reinforcing bars, as mentioned in Eqs. (6) and (10). The ultimate strain deterioration of confined core concrete due to corrosion can be simply estimated

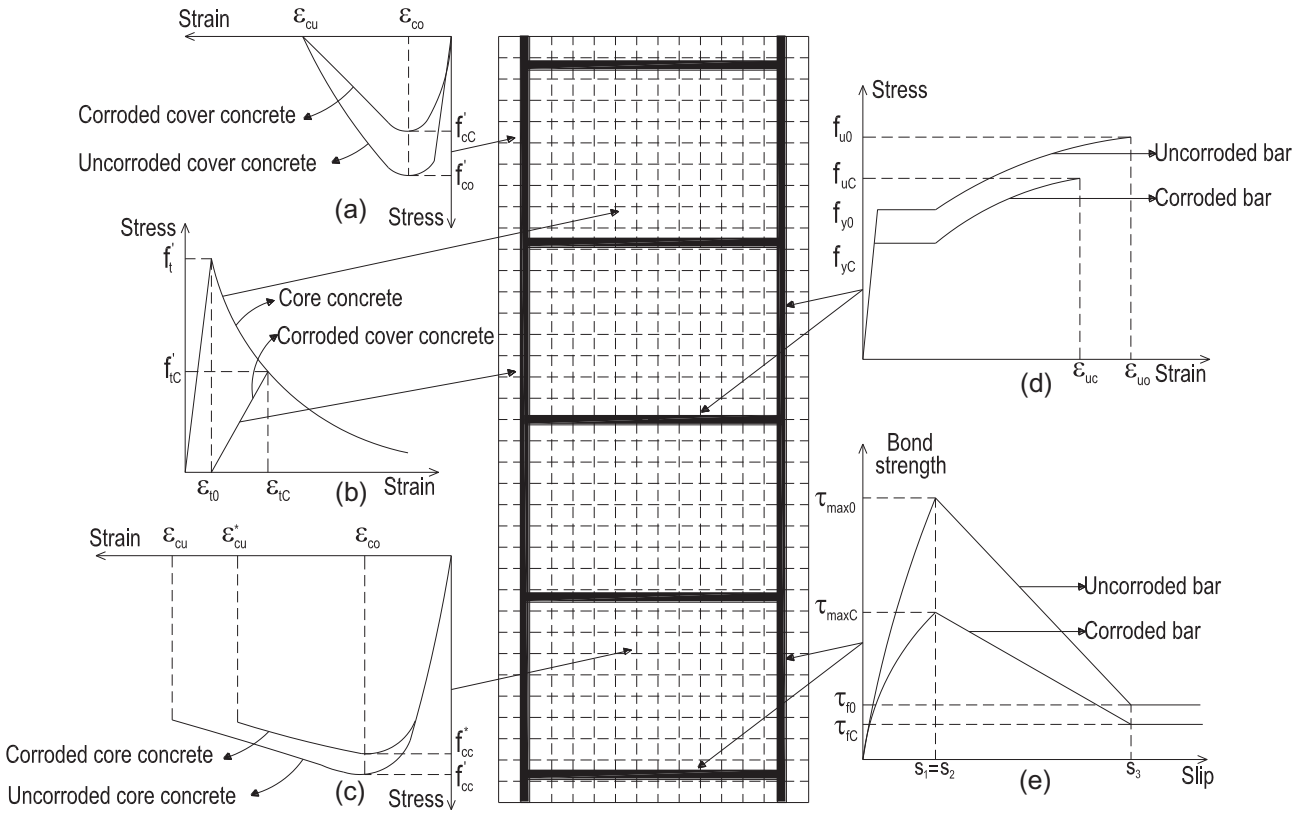

Fig. 2. Column FE model – Constitutive models for: (a) Cover concrete under compression and (b) Tension; (c) Confined core concrete under compression; (d) Steel reinforcement; (e) Local bond stress-slip relationship.

using Eq. (13) by altering the yield strength f_{yh} and ultimate strain ε_{uc} of transverse reinforcement according to Eqs. (10) and (11), respectively. Fig. 2(c) presents the modeling of uncorroded and corroded confined concrete under compression.

2.5. Modified bond deterioration model

2.5.1. Bond strength of corroded reinforcement

Various bond strength deterioration models of corroded reinforcement induced by corrosion are available in literature [26–28]. In this paper, the bond strength model developed by Maaddawy et al. [29] is utilized to calculate the maximum bond strength of corroded reinforcement. As compared to other empirical bond strength models, some advantages of this model include its ability to take into account the contributions from concrete and stirrup independently and also consider the effect of impressed current density for accelerated corrosion on the bond strength deterioration. In this model, the maximum bond stress of corroded reinforcement $\tau_{max\,C}$ can be expressed as follows:

$$\tau_{max\,C} = R\left(0.55 + 0.24\frac{c_c}{d_b}\right)\sqrt{f'_c} + 0.191\frac{A_v f_{yh}}{Sd_b} \tag{14}$$

$$R = (A_1 + A_2 X_{corr}) \tag{15}$$

where R is the empirical factor that predicts the change of bond strength induced by corrosion of reinforcement.A_1 and A_2 are the variables that depend on the current density used for accelerated corrosion, for details see [29].

2.5.2. Modified local bond stress-slip model

To take consideration the influence of corrosion on the local bond behavior, the bond stress-slip model developed in the CEB-FIP [18] is utilized and modified by using Eq. (14) as:

$$\begin{aligned}
&\tau = \tau_{max\,C}\left(\tfrac{s}{s_1}\right)^{\alpha} && \text{For } 0 \leqslant s \leqslant s_1\\
&\tau = \tau_{max\,C} && \text{For } s_1 \leqslant s \leqslant s_2\\
&\tau = \tau_{max\,C} - (\tau_{max\,C} - \tau_f)\left(\tfrac{s-s_2}{s_3-s_2}\right) && \text{For } s_2 \leqslant s \leqslant s_3\\
&\tau = \tau_f && \text{For } s_3 < s
\end{aligned} \tag{16}$$

It is noted that with the generally designed cover concrete thickness and transverse reinforcement amount, the bond failure in corroded reinforcement is mostly due to splitting [19]. Therefore, the values of parameters of the modified bond stress-slip model can be chosen as:

$$\alpha = 0.4; \quad s_1 = 0.6\text{ mm}; \quad s_2 = 0.6\text{ mm}; \quad s_3 = 2.5\text{ mm};$$
$$\tau_f = 0.15\tau_{max\,C} \tag{17}$$

Fig. 2(e) shows an example of the modified bond model for uncorroded and corroded reinforcing bars.

3. Validation of proposed 3D non-linear FE model

Three experimental studies reported in literature [10,12,13] on the performance of corroded RC columns under the simulated seismic loading are selected to validate the accuracy of the proposed 3D non-linear FE model. The first experimental study carried out by Wang [10] comprised 17 RC columns owing the same specifications, which were subjected to different axial force ratios from 0 to 0.5 and varying corrosion levels. In this experimental program, both longitudinal and transverse reinforcing bars were corroded until the expected corrosion levels from 0 to 25% in terms of mass loss. In the second experimental study conducted by Goksu [12], 13 RC columns were accelerated corrosion in which the corrosion level varies from 0 to 54%, and then tested as singer curvature under constant axial force ratio of 0.18 together with cyclic loading. The last experimental study

conducted by Meda et al. [13] includes four RC columns with the same specifications in which the first two columns were accelerated corrosion, and then the reinforcement was extracted from these RC columns and tested in tension to study about the corrosion effect on the stress-strain relationships of corroded reinforcement. The third column was corroded up to a desired corrosion level of approximately 20% and subjected to cyclic loading while the last column was used as reference uncorroded specimen for comparison against the corroded RC column. It is noted that in the second and third experimental studies [12,13], only longitudinal reinforcing bars were corroded.

In total, the experimental data of 9 RC columns in three experimental studies were selected to validate the proposed 3D non-linear FE model, in which both uncorroded and corroded RC columns as well as various corrosion levels were examined. The details of these RC column specimens are shown in Table 1 and Fig. 3 while their material properties used in the 3D non-linear FE analyses are indicated in Table 2. Figs. 4–6 indicate the comparison of hysteresis loops between the numerical analyses and the experimental data for both uncorroded and corroded RC columns in these three experimental studies. As observed, there is a good correlation in the overall global behavior between the experimental and FE results in terms of the initial stiffness, energy dissipation capacity, lateral load resistance, and ultimate displacement. To quantify the accuracy of the FE analyses, the normalized hysteretic force error E_{force} and normalized hysteretic energy error E_{energy} are evaluated; those are the errors between measured and calculated hysteretic forces and hysteretic energies, respectively, as the following equations [30]:

$$E_{force} = \frac{1}{\max(|F_{mea}|)}\sqrt{\frac{1}{n}\sum_{i=1}^{n}(F_{mea}^{i} - F_{cal}^{i})^{2}} \tag{18}$$

$$E_{energy} = \frac{\Omega_{mea} - \Omega_{cal}}{\Omega_{mea}} \tag{19}$$

$$\Omega = \sum_{i=1}^{n-1}\frac{F_{i+1} - F_{i}}{2}(\Delta_{i+1} - \Delta_{i}) \tag{20}$$

where F_{mea} and F_{cal} are the measured and calculated lateral forces at corresponding displacements; F_i and Δ_i are the lateral force and horizontal displacement at the i^{th} step; Ω_{mea} and Ω_{cal} are the measured and calculated areas within the hysteresis loops which can be estimated based on the trapezoid numerical integration scheme as Eq. (20). It is noted that if the hysteretic energy $E_{energy} < 0$, the estimated response overestimates the amount of dissipated energy in the experiment, otherwise it is underestimated if the hysteretic energy $E_{energy} > 0$.. Table 3 summarizes the values of normalized hysteretic force error and normalized hysteretic energy error of 9 RC columns. As indicated, the mean error in hysteretic force is 10.53% and the mean absolute error in hysteretic energy is 5.92%. These values are lower than those reported by Lepech et al. [31] in their validation of corroded circular RC columns using OpenSees modeling software, those are 12.9% of mean error in hysteretic force and 25.3% of the mean absolute error in hysteretic energy, respectively.

In order to verify the applicability and accuracy of numerical models, Figs. 7 and 8 present the stress contour in reinforcement and concrete at the collapse of corroded RC columns tested by Meda et al. [13] and Goksu [12]. These figures also indicate the comparison of the crack pattern obtained from 3D non-linear FE analyses and the observed experimental crack pattern at the final stage of cyclic loading of these corroded RC columns. As shown in these figures, the most critical regions of forming cracks near the bottom of corroded RC columns in the experiment are predicted accurately in the 3D non-linear FE analyses.

The aforementioned verification of finite element results revealed that the proposed FE model is acceptable and can be adopted to predict the performance of corroded RC columns under seismic loading. Based on the well-estimated model, further numerical simulation and parametric study will be performed by varying critical parameters to estimate the lateral load resistance and ultimate drift capacity of corroded RC columns.

4. Parametric investigation

4.1. Numerical models of corroded RC columns

Adopting the proposed 3D non-linear FE model discussed above, numerical simulations were performed to study the influence of various parameters on the seismic behavior of corroded RC columns, and to further estimate the reduction of their lateral load resistance and ultimate drift ratio capacity. An extensive parametric study was carried out, including corrosion level, column aspect ratio, axial force ratio, transverse reinforcement ratio, and compressive concrete strength. Table 4 tabulates the range of studied parameters. The parametric investigation is conducted by analyzing the FE models of 12 RC columns, labeled from series A to series L, as indicated in Fig. 9. The series A, B, E, F, I and J columns are designed for seismic zones according to the requirement in the ACI 318-14 [32] with sufficient stirrup in the plastic hinge zone. Table 5 summarizes the specimen configurations in the parametric study.

4.2. Numerical results of corroded RC columns

4.2.1. Influence of corrosion level

The 3D non-linear FE analyses for the simulated models subjected to different corrosion levels are presented in this section. In reality, the corrosion level of transverse reinforcement is slightly larger than that of the longitudinal reinforcement due to its smaller diameter and its distance to the outside environment is nearer. However, to simplify the analyses, the longitudinal reinforcement

Table 1
Summary of RC column specimens to validate the proposed FE model.

Specimens	bxh (mm)	L (mm)	Aspect ratio	Longitudinal reinforcement	Transverse reinforcement	Axial force ratio	Corrosion level (%)
ZZ-1 [10]	200 × 200	1100	5.5	6Ø14	Ø6@80	0.34	0
XZ-2 [10]				$\rho_l = 2.31\%$	$\rho_v = 0.93\%$	0	6
XZ-7 [10]						0.25	4
Z-4 [10]						0.34	18
NS-X0 [12]	200 × 300	1260	5.5	4Ø14	Ø8@100	0.18	0
NS-X9 [12]				$\rho_l = 1.03\%$	$\rho_v = 1.08\%$		9
NS-X16 [12]							16
UC [13]	300 × 300	1800	5.33	4Ø16	Ø8@300	0.22	0
CC [13]				$\rho_l = 0.89\%$	$\rho_v = 0.27\%$		20

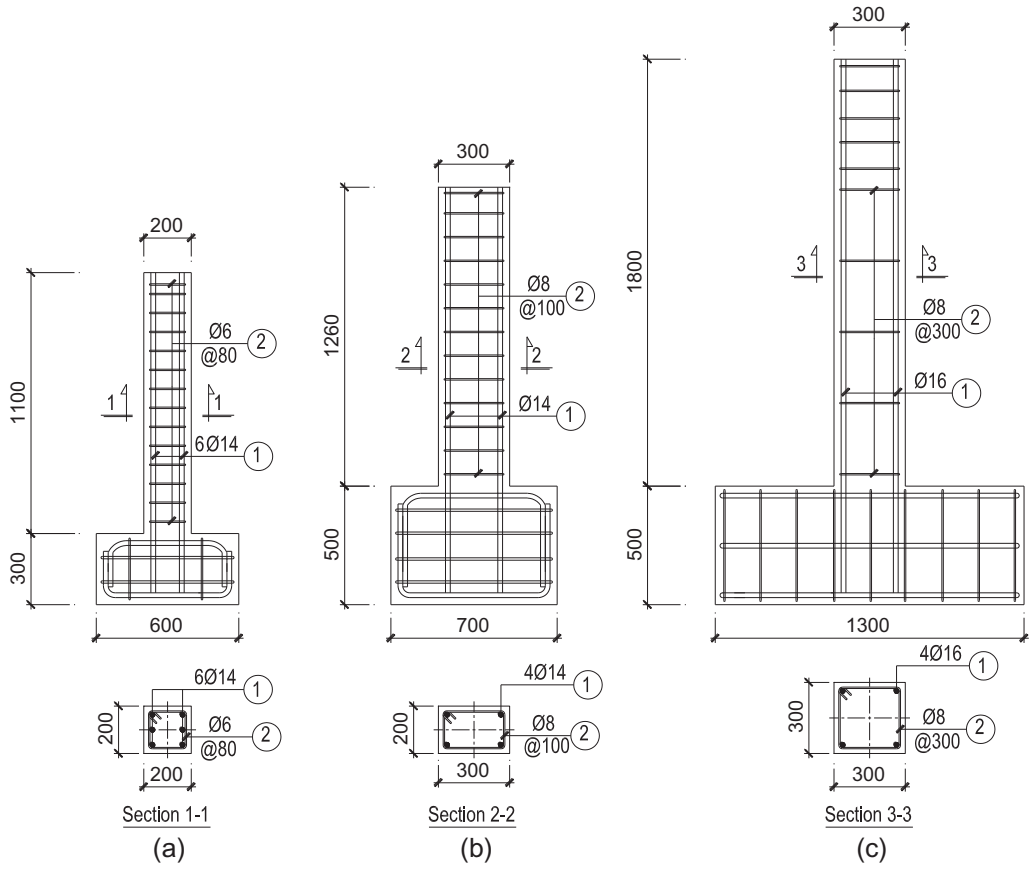

Fig. 3. Details of specimens tested by: (a) Wang [10]; (b) Goksu [12]; (c) Meda et al. [13].

Table 2
Material properties of RC column specimens in FE analyses.

Specimens	Cover concrete		Confined core concrete			Longitudinal reinforcement		Transverse reinforcement		τ_{max} MPa
	f_c' MPa	f_t' MPa	f_{cc}' MPa	f_t' MPa	ε_{cu}	f_y/f_u MPa/MPa	ε_u	f_y/f_u MPa/MPa	ε_u	
ZZ-1 [10]	24.56	2.53	28.2	2.53	0.026	415/639	0.15	325/565	0.15	6.43
XZ-2 [10]	16.35	1.69	27.7		0.022	412/634	0.123	322/560	0.123	5.35
XZ-7 [10]	18.42	1.90	28.0		0.024	414/637	0.132	324/563	0.132	5.71
Z-4 [10]	9.60	0.99	25.8		0.014	386/594	0.069	302/525	0.069	3.20
NS-X0 [12]	25.5	2.6	29.3	2.6	0.037	460/652	0.115	486/681	0.134	9.14
NS-X9 [12]	18.15	1.85				452/640	0.084			7.22
NS-X16 [12]	14.70	1.50				434/615	0.060			5.72
UC [13]	20.0	2.21	20.0	2.21	0.022	520/620	0.18	520/620	0.18	5.85
CC [13]	10.61	1.17				260/434	0.045			2.30

and transverse reinforcement are assumed to be corroded at the same level in the current parametric study. Fig. 10 demonstrates the effect of corrosion level on the backbone curve of lateral load-displacement relationships in which the corrosion level varies from 0% to 30%. As observed, the higher corrosion level results in the lower lateral load resistance and its significant reduction can be seen when the RC columns are highly corroded, that is the corrosion level from 20% to 30%. For example, the studied series E column with the axial force ratio of 0.2 and transverse reinforcement ratio of 1.07%, when the corrosion level increases from 0% to 5%, 10%, 20%, and 30%, the lateral load resistance reduces 6%, 12%, 21%, and 28%, respectively. The more serious deterioration of lateral load resistance in the series G column with axial force ratio of 0.4 and transverse reinforcement ratio of 0.64%, that is the decrease of 10%, 17%, 29%, and 39% can be seen with the rise of corrosion level from 0 to 5%, 10%, 20%, and 30%, respectively. Therefore, it is concluded that the corrosion effect on the lateral load resistance deterioration is more critical in cases of lower transverse reinforcement amount and higher axial force. With regard to the ultimate drift capacity, it appears that higher corrosion level results in the lower ultimate drift capacity. As observed in Fig. 10, the uncorroded series E column failed when the drift ratio reached 4.5% while this column with the corrosion level of 30% failed at the ultimate drift ratio of 3%. However, when the corrosion level is less than 10%, the ultimate drift ratio of the corroded series E and G columns is not significantly affected.

4.2.2. Influence of aspect ratio

In this paper, the width and depth of the RC column section are kept constant for all the 3D non-linear FE models. Therefore, an increase in the aspect ratio refers to an increase of total column height. The influence of aspect ratio on the backbone curves of corroded RC columns is demonstrated in Fig. 11 in which the aspect ratio varies from 2.0 to 3.0 and 4.0 to represent both

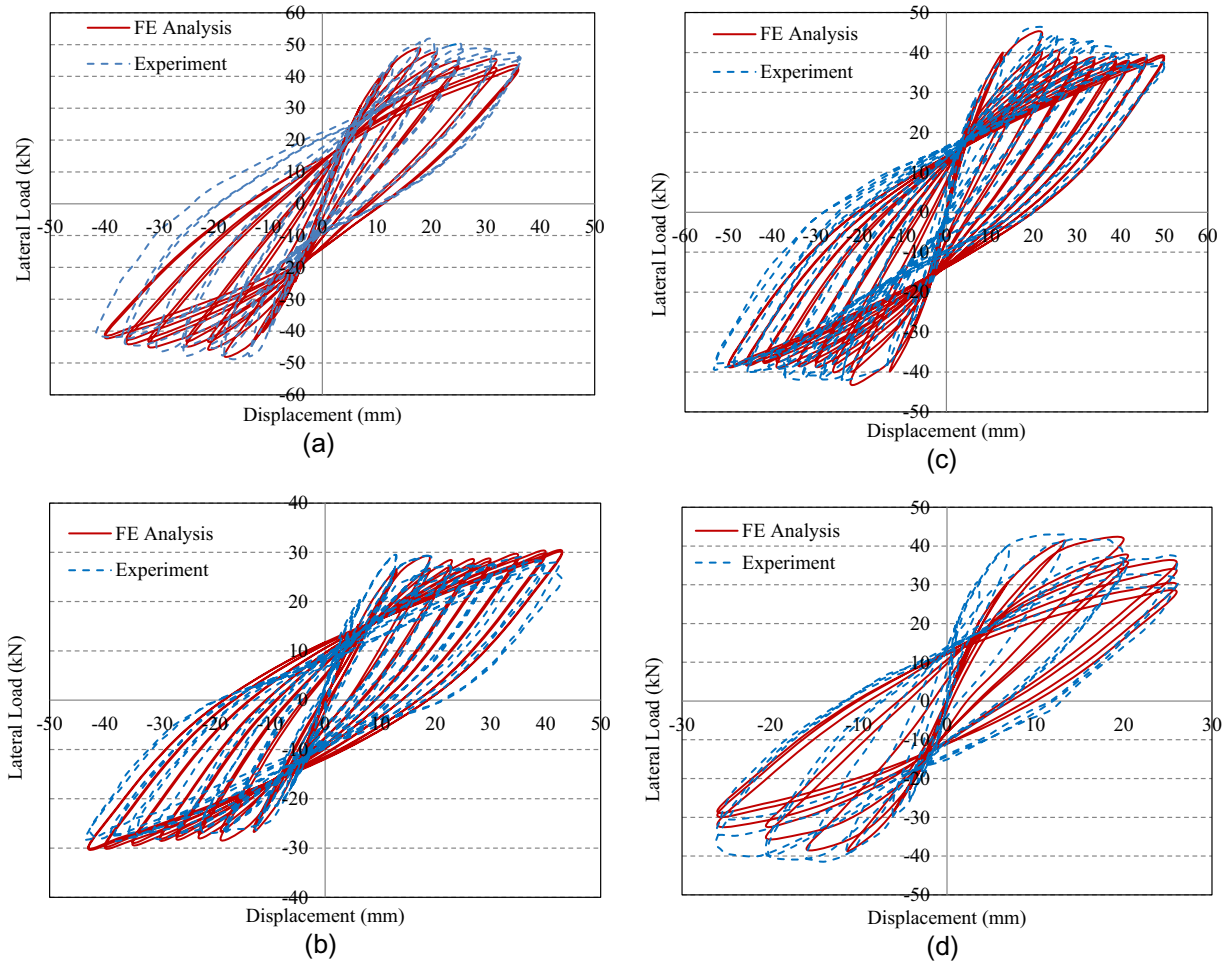

Fig. 4. Comparison of analyzed and experimental hysteresis loops of specimens tested by Wang [10]: (a) ZZ-1; (b) XZ-2; (c) XZ-7; (d) Z-4.

shear-critical and flexural RC columns. At the same corrosion level, with the increase of aspect ratio from 2.0 to 3.0 and 4.0, the lateral load resistance reduces by approximately 30% and 45%, respectively. On the other hand, the increase of aspect ratio results in the higher ultimate drift capacity of corroded RC columns, for instance, the series C, G, and K columns with the corrosion level of 20% and axial force ratio of 0.2 failed at the ultimate drift ratio of 2.0%, 2.5% and 3% in which the aspect ratio varies from 2.0 to 3.0 and 4.0, respectively. Therefore, it is concluded that among the 3D non-linear FE models with the same corrosion level, the higher aspect ratio results in the higher ductility capacity. However, the lower lateral load resistance is obtained in these FE models with the higher aspect ratio.

4.2.3. Influence of axial force ratio

It is well-known that the axial force is considered as one of the key parameters in the studies of seismic behavior of RC columns. However, its effect on the corroded RC columns is still scarce in literature in terms of both experimental and analytical studies. In this paper, the axial force ratio varies from 0.1 to 0.4. Fig. 12 indicates that the lateral load resistance of corroded columns rises with an increase in axial force, for example, the corroded series C column subjected to the corrosion level of 30%, the lateral load resistance rises by approximately 12%, 16%, and 19% when the axial force ratio increases from 0.1 to 0.2, 0.3, and 0.4, respectively. In contract, the higher axial force causes a more brittle behavior in corroded RC columns. As indicated in the series I column with the corrosion level of 10%, these corroded RC columns failed at the ultimate drift ratio of 4.5%, 3.5%, 3%, and 2.5% corresponding to the axial force ratio varies from 0.1 to 0.2, 0.3, and 0.4, respectively.

4.2.4. Influence of volumetric transverse reinforcement ratio

Generally, the stirrup amount and distribution play a vital role in improving the strength and ductility capacity of RC columns because of its confinement effect [33]. Fig. 13 demonstrates the effect of stirrup amount on the performance of corroded RC columns. As observed in the studied series I & K columns subjected to the axial force ratio of 0.3, an approximately 10% and 16% lateral load resistance decrease is observed for corroded RC columns with corrosion level of 10% and 30%, respectively corresponding to the reduction of the volumetric transverse reinforcement ratio from 1.07% to 0.64%. It is also revealed that the effect of transverse reinforcement amount on the lateral load resistance deterioration of corroded RC columns becomes more significant in cases of higher corrosion level. Furthermore, the ultimate drift capacity significantly decreases in cases of corroded RC columns with lower transverse reinforcement amount. For example, the ultimate drift ratio of series A & C columns under axial force ratio of 0.2 and corrosion level of 20%, with a decrease of volumetric transverse reinforcement ratio from 1.07% to 0.64%, the ultimate drift ratio reduces from 3.5% to 2.5%, respectively. In conclusion, the volumetric transverse reinforcement ratio drastically influences both the lateral load resistance and ultimate drift capacity of corroded RC columns.

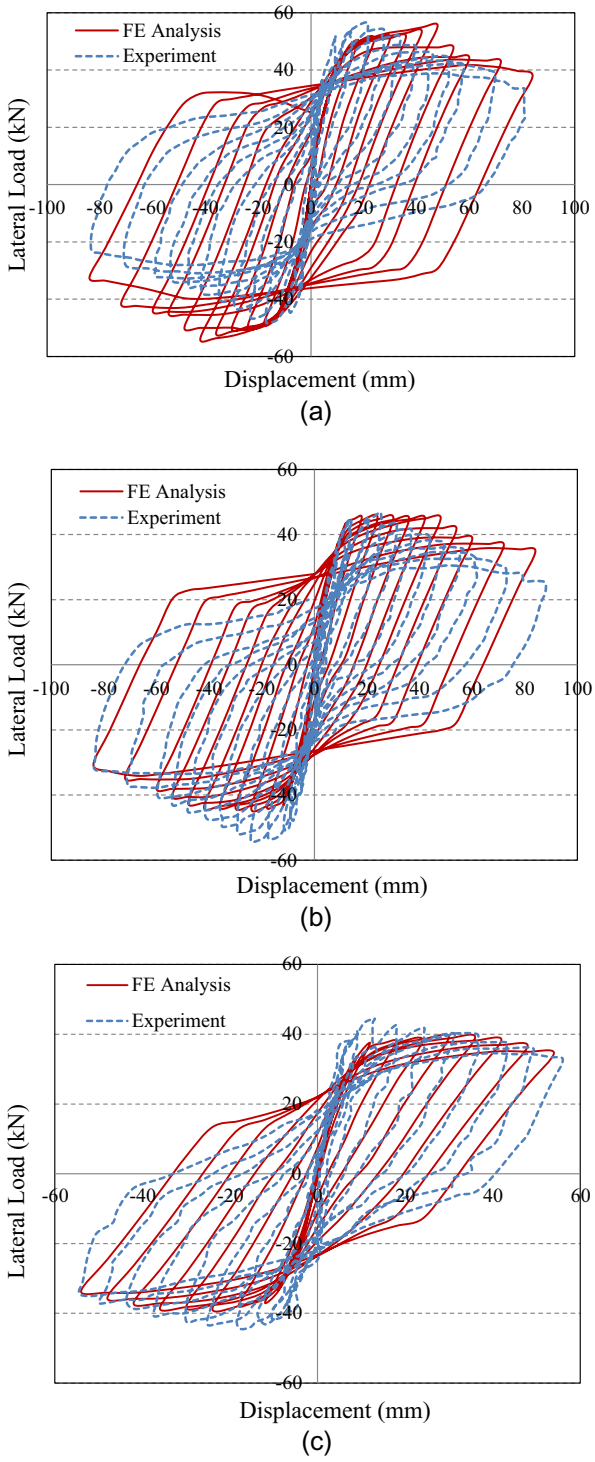

Fig. 5. Comparison of analyzed and experimental hysteresis loops of specimens tested by Goksu [12]: (a) NS-X00; (b) NS-X09; (c) NS-X16.

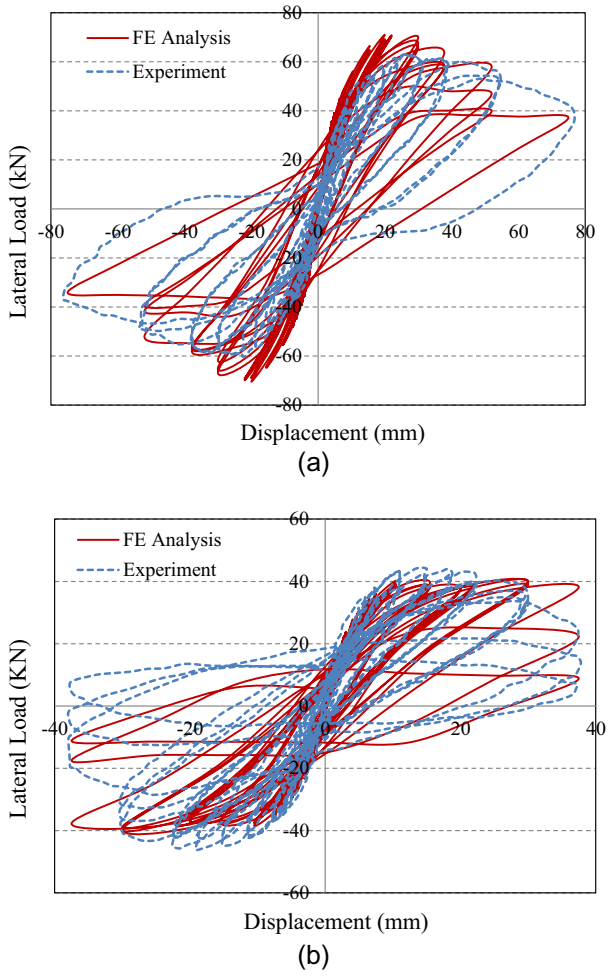

Fig. 6. Comparison of analyzed and experimental hysteresis loops of specimens tested by Meda et al. [13]: (a) Uncorroded column – UC; (b) Corroded column – CC ($X_{corr} = 20\%$).

Table 3
Summary of normalized hysteretic force error and normalized hysteretic energy error of RC column specimens in FE validation.

Specimens	Normalized hysteretic force error E_{force} (%)	Normalized hysteretic energy error E_{energy} (%)
ZZ-1 [10]	7.73	3.81
XZ-2 [10]	5.15	−4.56
XZ-7 [10]	8.73	5.05
Z-4 [10]	10.11	3.90
NS-X0 [12]	15.60	−12.64
NS-X9 [12]	12.43	5.21
NS-X16 [12]	9.13	3.16
UC [13]	13.75	−11.35
CC [13]	12.16	−3.61
Mean absolute error	10.53	5.92

4.2.5. Influence of compressive concrete strength

Fig. 14 demonstrates the effect of compressive concrete strength on the performance of corroded RC columns. The FE results revealed that at the same corrosion level, the lateral load resistance of corroded RC columns increases along with the compressive concrete strength. For example, the studied series G & H columns subjected to corrosion level of 20% and axial force ratio of 0.2, when the compressive concrete strength increases from 30 MPa to 40 MPa, the lateral load resistance rises by approximately 16% and the similar tendencies can be seen for other corrosion levels. However, regarding to the ultimate drift capacity, with a rise of compressive concrete strength from 30 MPa to 40 MPa, no significant changes were observed on the corroded RC columns subjected to the same corrosion level.

4.3. Prediction of lateral load resistance and ultimate drift capacity for corroded RC columns

4.3.1. Prediction equation of lateral load resistance

The parametric study on 240 FE models was carried out to reveal the significance of several key parameters that influence

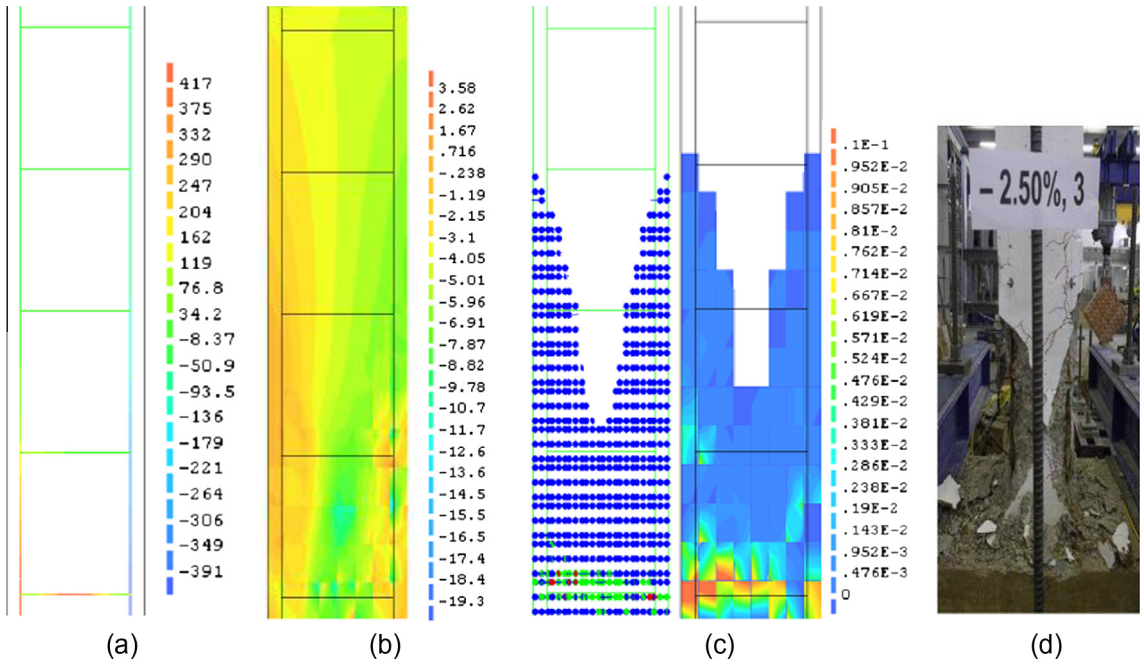

Fig. 7. Finite element analyses of the corroded RC column (CC) at the final stage of cyclic loading tested by Meda et al. [13]: (a) Stress in reinforcement; (b) Concrete normal stress contour; (c) Crack pattern and crack strain; (d) Observed experimental crack pattern.

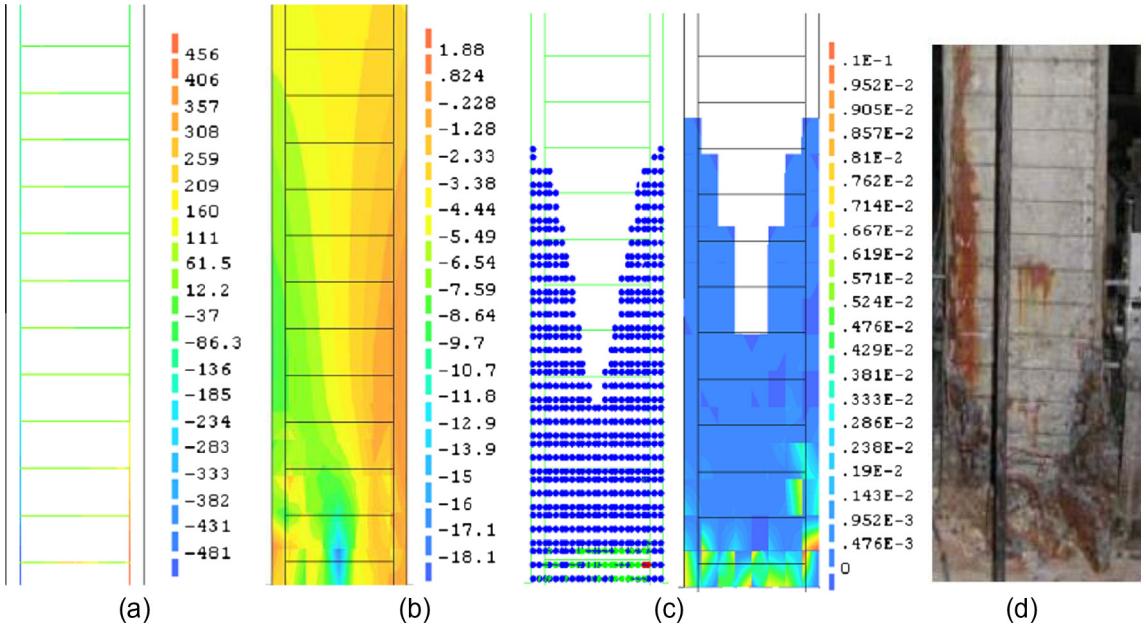

Fig. 8. Finite element analyses of the corroded RC column (NS-X16) at the final stage of cyclic loading tested by Goksu [12]: (a) Stress in reinforcement; (b) Concrete normal stress contour; (c) Crack pattern and crack strain; (d) Observed experimental crack pattern.

Table 4
Parameters study.

No.	Notation	Description	Range investigated
1	$X_{corr}(\%)$	Corrosion level	0, 5, 10, 20, 30
2	a/d	Aspect ratio	2.0, 3.0, 4.0
3	N/f'_cA_g	Axial force ratio	0.1, 0.2, 0.3, 0.4
4	ρ_v (%)	Volumetric transverse reinforcement ratio	0.64, 1.07
5	f'_c (MPa)	Compressive concrete strength	30, 40

the lateral load resistance deterioration of corroded RC columns under cyclic loading, particularly corrosion level, column aspect ratio, axial force ratio, volumetric transverse reinforcement ratio, and compressive concrete strength. Comparison between the FE analysis results of lateral load resistance of 48 uncorroded RC column models and their shear strength calculated by equation in the ASCE 41-06 [34] shows that the numerical results produced a good agreement with the shear strength prediction in the ASCE 41-06 [34], as demonstrated in Fig. 15, particularly the average of ratio of their strength calculated from the equation in the ASCE 41-06 [34] to numerical results is equal to 1.05 and its standard

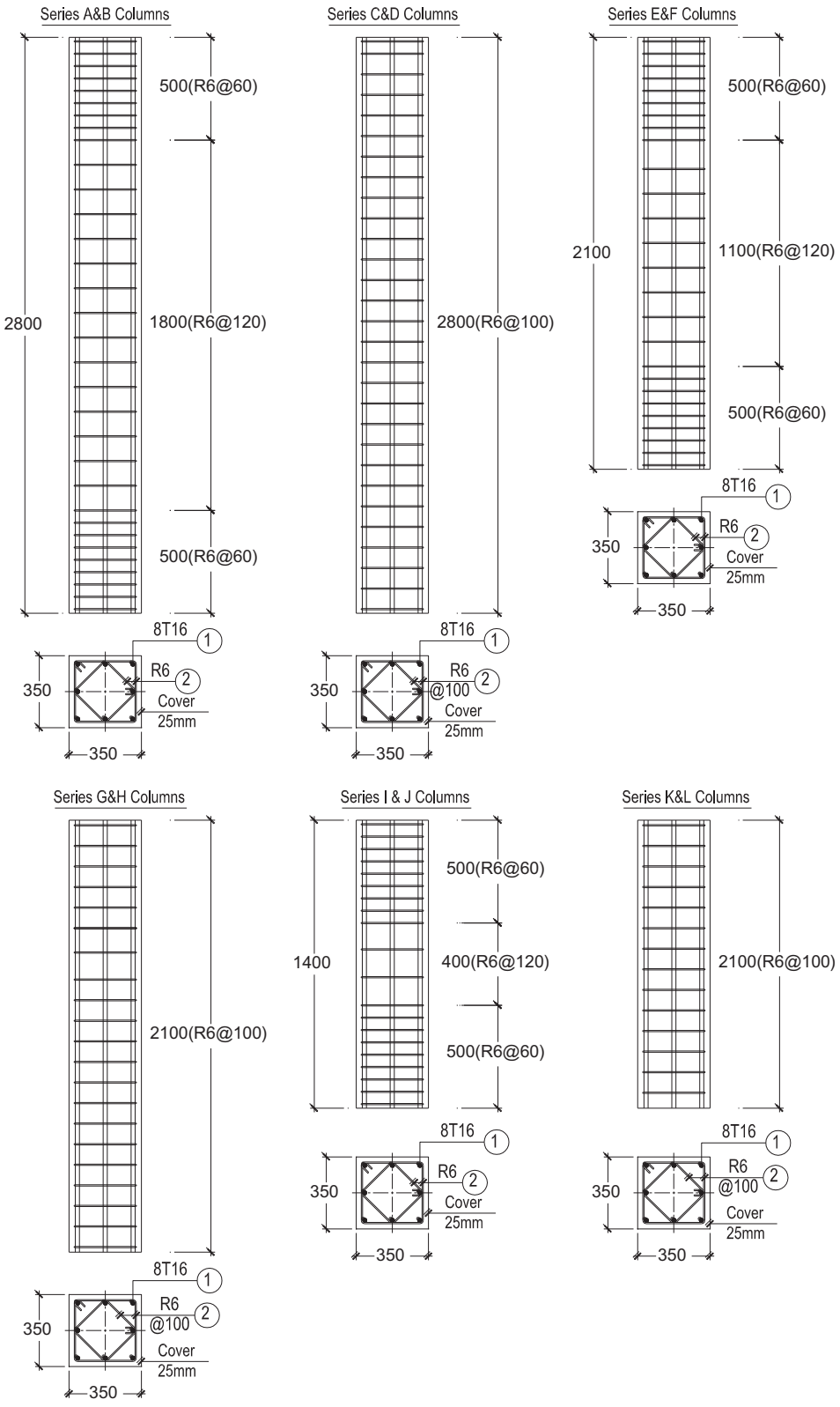

Fig. 9. Details of specimens in the parametric study.

deviation of 0.16. Therefore, in this study the shear strength equation proposed in the ASCE 41-06 [34] is adopted and modified to calculate the lateral load resistance of corroded RC columns. By conducting the regression analysis of the numerical results of 240 FE models, the prediction equation of the lateral load resistance for corroded RC columns is derived as follows:

$$V_{nC} = \left(\frac{1}{1+1.59\frac{X_{corr}}{100}}\right)\left(\frac{0.7A_v f_{yh} d}{S} + \frac{0.35\sqrt{f'_c}}{a/d}\sqrt{1+\frac{N}{0.5\sqrt{f'_c}A_g}}0.8A_g\right) \quad (21)$$

Table 5
Characteristics of the specimens in the parametric study.

Series column	Width & depth *bxh* mm	Column height *L* mm	Aspect ratio *a/d*	Concrete strength f'_c MPa	Longitudinal reinforcement		Transversereinforcement	
					ρ_l %	f_{yo}/f_{uo} MPa/Mpa	ρ_v%	f_{yo}/f_{uo} MPa/Mpa
A	350 × 350	2800	4.0	30	1.31	400/550	1.07	400/550
B				40			1.07	
C				30			0.64	
D				40			0.64	
E	350 × 350	2100	3.0	30			1.07	
F				40			1.07	
G				30			0.64	
H				40			0.64	
I	350 × 350	1400	2.0	30			1.07	
J				40			1.07	
K				30			0.64	
L				40			0.64	

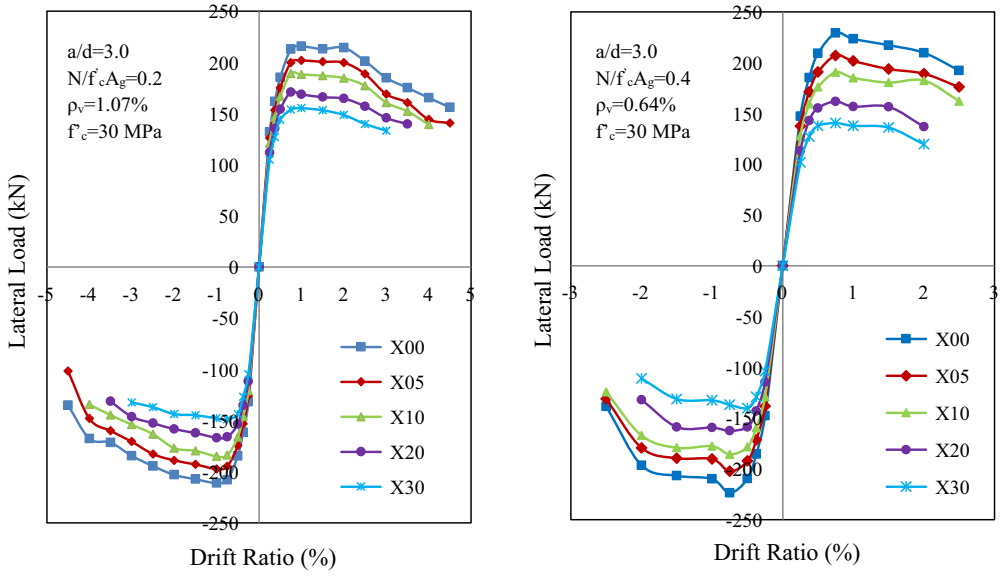

Fig. 10. Influence of corrosion level on the backbone curve of corroded RC columns.

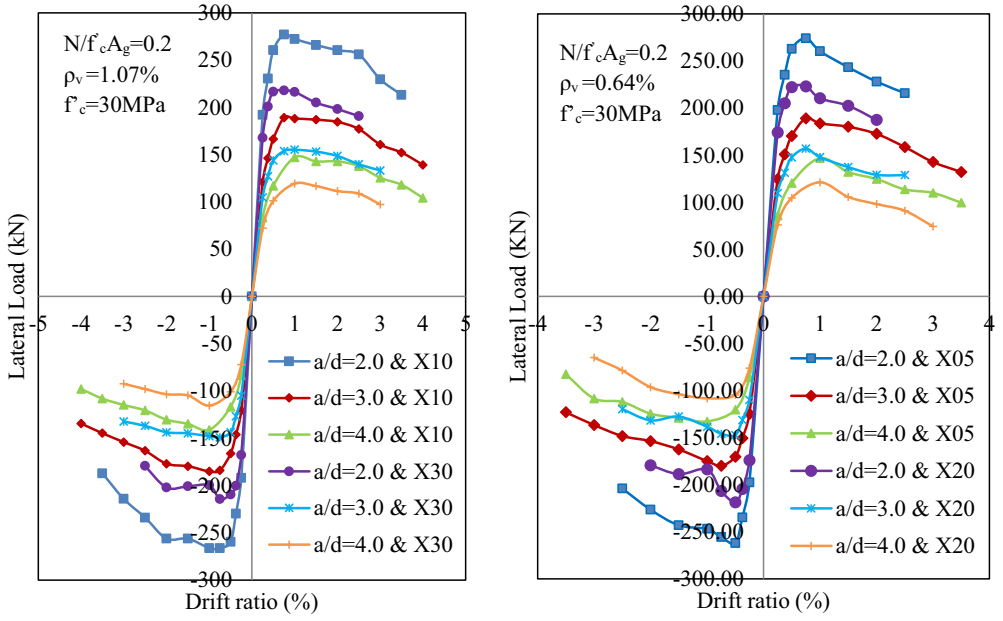

Fig. 11. Influence of aspect ratio on the backbone curve of corroded RC columns.

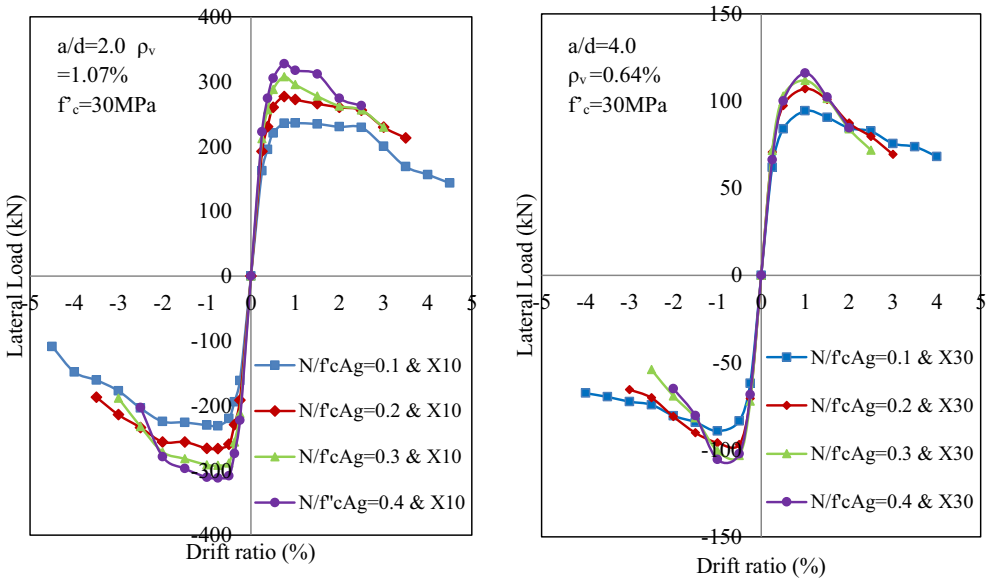

Fig. 12. Influence of axial force ratio on the backbone curve of corroded RC columns.

where V_{nC} is the lateral load resistance of the corroded RC column; X_{corr} is the corrosion level. The average ratio of the lateral load resistance of 240 FE models calculated by FE analyses to their lateral load resistance predicted by adopting Eq. (21) is 0.974 and its standard deviation of 0.083, showing a good correlation between the FE analyses and this prediction equation, as illustrated in Fig. 16. In addition, the lateral load resistance of 25 tests of uncorroded and corroded RC columns calculated by Eq. (21) is then compared to the experimental results. As shown in Table 6, the comparison shows a good agreement between the experimental data and the proposed equation because the average lateral load resistance ratio of the experiment to the prediction using Eq. (21) is 0.962 and its standard deviation of 0.260.

4.3.2. Prediction equation of ultimate drift capacity

Ultimate drift capacity of the RC column is usually studied using lateral load-displacement responses. As the common practice in literature, the ultimate lateral displacement capacity of a RC column can be defined as a displacement value corresponding to the maximum lateral load carrying capacity deteriorates 20% [35–38]. Several studies have proposed drift-based design equations for RC columns in which the effect of the confinement coefficient mainly due to the stirrup amount and distribution, aspect ratio and axial force has been incorporated into these equations [35,39,40]. However, the influence of reinforcement corrosion on the ultimate drift capacity deterioration of corroded RC columns has not been well studied. The numerical results mentioned above revealed the significance of several key factors that influence the ultimate drift capacity of corroded RC columns, such as corrosion level, aspect ratio, axial force ratio, and transverse reinforcement ratio. Therefore, based on the multivariable regression analysis of numerical results of 240 FE models, the prediction equation of the ultimate drift capacity of corroded RC columns subjected to the simulated seismic loading is proposed as follows:

$$DR_{ultC} = \left(\frac{1}{1+1.88\frac{X_{corr}}{100}}\right)(0.45+0.21\rho_v)\left(1.66+\frac{0.26}{\frac{N}{f'_cA_g}}\right)\left(1.49+0.12\frac{a}{d}\right) \quad (22)$$

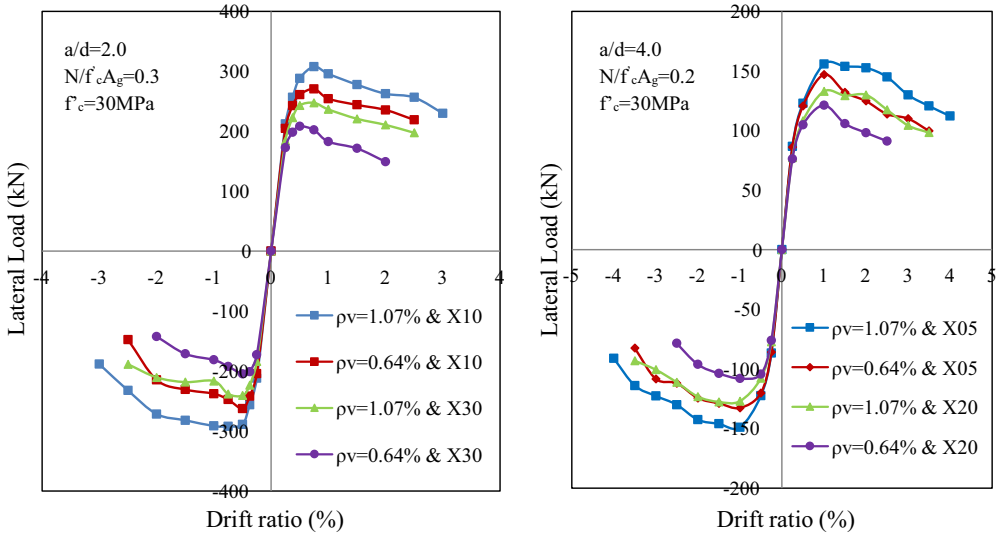

Fig. 13. Influence of volumetric transverse reinforcement ratio on the backbone curve of corroded RC columns.

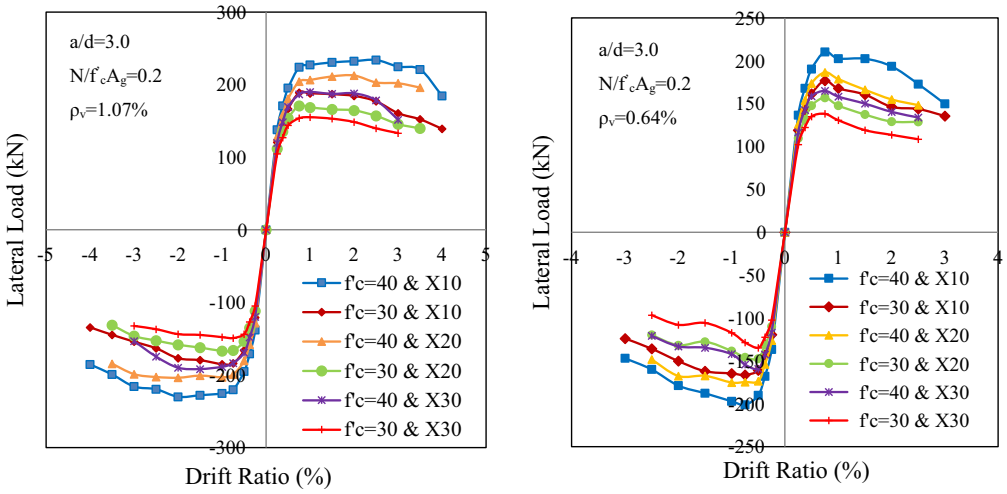

Fig. 14. Influence of compressive concrete strength on the backbone curve of corroded RC columns.

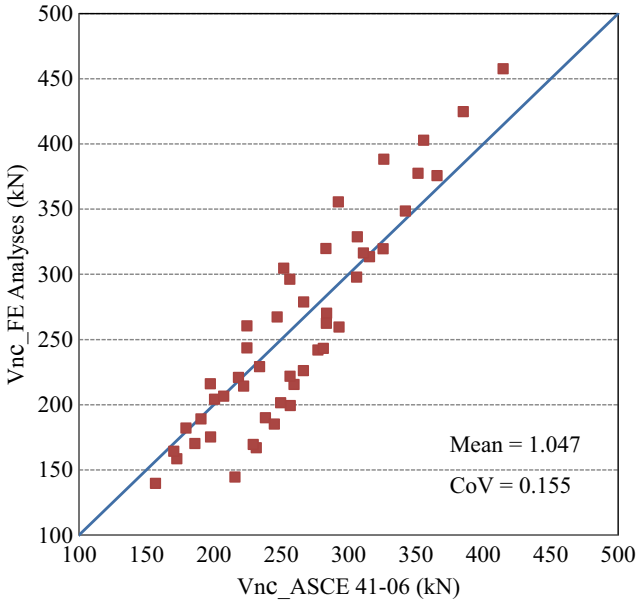

Fig. 15. Comparisons of the lateral load resistance of 48 uncorroded RC column models between calculated by FE analyses and ASCE 41-06 [34].

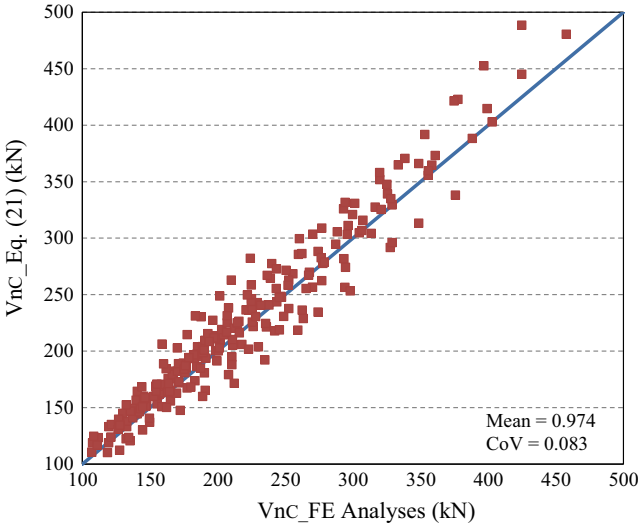

Fig. 16. Comparisons of the lateral load resistance of 240 FE models between calculated by FE analyses and Eq. (21).

where DR_{ultC} is the ultimate drift capacity of the corroded RC column; X_{corr} is the corrosion level which can be estimated based on Eq. (7) or Eq. (8). The comparison between the FE analyses and the proposed equation produces a good correlation because the average ratio of ultimate drift ratio of 240 FE models calculated by FE analyses to their ultimate drift ratio predicted by adopting Eq. (22) is 0.996 and its standard deviation of 0.137, as demonstrated in Fig. 17. Furthermore, the applicability of this proposed equation for prediction of ultimate drift capacity of corroded RC columns is verified by comparing to the experimental results of 21 tests in literature. Table 6 shows the average ratio of the experimental to the predicted ultimate drift capacity of corroded RC columns by using Eq. (22) is 1.086 and its standard deviation of 0.114.

5. Conclusions

In this paper, the influences of reinforcement corrosion on the seismic behavior of RC columns are studied using the 3D non-linear FE approach. The critical parameters influencing the performance of corroded RC columns are investigated and their effects as well as interaction on the lateral load resistance and ultimate drift capacity of corroded RC columns are quantified, including corrosion level, aspect ratio, axial force ratio, concrete compressive strength, and transverse reinforcement ratio. According to the numerical results, some important conclusions can be summarized:

1. The 3D non-linear FE model for the corroded RC columns subjected to the seismic loading was proposed that considers the degradation of corroded materials, including reduction in strength and ductility of both unconfined cover concrete and confined core concrete, decrease of cross-sectional area, strength and ultimate strain of corroded reinforcement, and bond strength deterioration of corroded reinforcement as well as modification of its local bond behavior.
2. The numerical analyses revealed that the lateral load resistance and ultimate drift capacity of corroded RC columns deteriorate when the corrosion level increases. The deterioration is more significant in RC columns subjected to higher corrosion levels

Table 6
Experimental verification of proposed equations of corroded RC columns.

	Specimen	X_{corr} (%)	f'_c (MPa)	f_{yh} (mm)	A_v (mm)	S (mm)	ρ_v (%)	$\frac{N}{f'_c A_g}$	$\frac{a}{d}$	V_{nC}^{exp} kN	V_{nC}^{pro} kN	DR_{ultC}^{exp} (%)	DR_{ultC}^{pro} (%)	$\frac{V_{nC}^{exp}}{V_{nC}^{pro}}$	$\frac{DR_{ultC}^{exp}}{DR_{ultC}^{pro}}$
Wang [10]	XZ-1	8	24.56	325	56.54	80	0.93	0.5	5.5	51.57	44.67	3.0	2.63	1.154	1.141
	XZ-2	6	24.56	325	56.54	80	0.93	0	5.5	29.50	32.70	4.0	–	0.902	–
	XZ-3	8	24.56	325	56.54	80	0.93	0	5.5	28.50	31.78	4.5	–	0.897	–
	XZ-4	9	24.56	325	56.54	80	0.93	0	5.5	29.10	31.33	4.5	–	0.929	–
	XZ-5	5	24.56	325	56.54	80	0.93	0.5	5.5	57.40	46.65	3.0	2.76	1.231	1.085
	XZ-6	5	24.56	325	56.54	80	0.93	0	5.5	30.00	33.18	3.0	–	0.904	–
	XZ-7	4	24.56	325	56.54	80	0.93	0.25	5.5	44.50	41.88	4.5	3.48	1.062	1.292
	XZ-8	6	24.56	325	56.54	80	0.93	0.25	5.5	44.00	40.67	4.5	3.37	1.082	1.337
	XZ-9	7	24.56	325	56.54	80	0.93	0.25	5.5	42.30	40.08	4.0	3.31	1.055	1.208
	XZ-10	6	24.56	325	56.54	80	0.93	0.5	5.5	53.80	45.97	3.3	2.72	1.170	1.214
	ZZ-1	0	24.56	325	56.54	80	0.93	0.34	5.5	51.90	46.82	3.3	3.36	1.108	0.981
	Z-2	14.5	24.56	325	56.54	80	0.93	0.34	5.5	47.00	38.05	3.0	2.64	1.235	1.135
	Z-3	16	24.56	325	56.54	80	0.93	0.34	5.5	43.50	37.33	2.5	2.59	1.165	0.967
	Z-4	18	24.56	325	56.54	80	0.93	0.34	5.5	41.90	36.40	2.5	2.51	1.151	0.995
	Z-5	24	24.56	325	56.54	80	0.93	0.34	5.5	40.80	33.89	2.0	2.32	1.204	0.863
	Z-6	6	24.56	325	56.54	80	0.93	0.34	5.5	55.90	42.74	3.5	3.02	1.308	1.158
	Z-7	19	24.56	325	56.54	80	0.93	0.34	5.5	45.00	35.96	2.0	2.48	1.251	0.807
Goksu [12]	NS-X00	0	25.5	486	100.5	100	1.08	0.18	5.5	56.90	107.95	5.0	4.52	0.527	1.107
	NS-X09	9	25.5	486	100.5	100	1.08	0.18	5.5	54.44	94.44	4.5	3.86	0.576	1.165
	NS-X13	13	25.5	486	100.5	100	1.08	0.18	5.5	42.39	89.46	3.0	3.63	0.474	0.826
	NS-X16	16	25.5	486	100.5	100	1.08	0.18	5.5	44.80	86.06	4.0	3.47	0.521	1.152
	NS-X22	22	25.5	486	100.5	100	1.08	0.18	5.5	46.01	79.97	4.0	3.20	0.575	1.252
	NS-X54	54	25.5	486	100.5	100	1.08	0.18	5.5	40.32	58.08	2.0	2.24	0.694	0.892
Meda et al. [13]	UC	0	20	520	100.5	300	0.27	0.22	5.33	63.00	65.69	3.5	3.07	0.959	1.141
	CC	20	20	520	100.5	300	0.27	0.22	5.33	46.00	49.84	2.5	2.23	0.923	1.122
											Mean			0.962	1.088
											Coefficient of variation			0.260	0.151

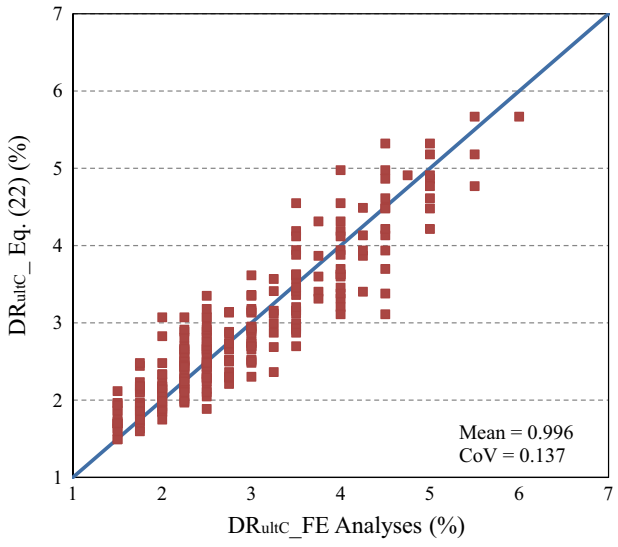

Fig. 17. Comparisons of the ultimate drift ratio capacity of 240 FE models between calculated by FE analyses and Eq. (22).

(20–30%) than those under low corrosion levels (0–10%). Furthermore, the FE results exposed that the influence of the corrosion level on the lateral load resistance deterioration is more significant in RC columns designed with lower stirrup amount and subjected to higher axial force. However, the ultimate drift capacity of corroded RC columns is not significantly affected when the corrosion level is less than 10%.

3. The FE results showed that the lateral load resistance of corroded RC columns reduces with the increase of aspect ratio, decrease of axial force ratio, and reduction in compressive concrete strength as well as stirrup amount. Furthermore, the effect of stirrup amount on the lateral load resistance deterioration becomes more significant in cases of RC columns subjected to the higher corrosion level. In contract, the ultimate drift capacity decreases with the reduction of aspect ratio, increase of axial force ratio, and decrease in transverse reinforcement ratio. However, it is not correlated with the change of compressive concrete strength.
4. Based on an extensive parametric investigation of various key parameters, two prediction equations of the lateral load resistance and ultimate drift capacity of corroded RC columns under the seismic loading were derived from the multivariable regression analysis of the numerical results of 240 FE models. Future experimental studies on the seismic performance of corroded RC columns are desired that will provide additional data to further verify the accuracy of the proposed 3D non-linear FE model and two prediction equations.

References

[1] Y.-C. Ou, H.-D. Fan, N.D. Nguyen, Long-term seismic performance of reinforced concrete bridges under steel reinforcement corrosion due to chloride attack, Earthquake Eng. Struct. Dynam. 42 (2013) 2113–2127.
[2] M.G. Stewart, Mechanical behaviour of pitting corrosion of flexural and shear reinforcement and its effect on structural reliability of corroding RC beams, Struct. Saf. 31 (2009) 19–30.
[3] Y.G. Du, L.A. Clark, A.H.C. Chan, Residual capacity of corroded reinforcing bars, Mag. Concr. Res. 57 (2005) 135–147.
[4] Y.G. Du, L.A. Clarkt, A.H.C. Chan, Effect of corrosion on ductility of reinforcing bars, Mag. Concr. Res. 57 (2005) 407–419.
[5] H.-S. Lee, S.-H. Cho, Evaluation of the mechanical properties of steel reinforcement embedded in concrete specimen as a function of the degree of reinforcement corrosion, Int. J. Fract. 157 (2009) 81–88.
[6] J. Cairns, G.A. Plizzari, Y. Du, D.W. Law, C. Franzoni, Mechanical properties of corrosion-damaged reinforcement, Mater. J. (2005) 102.
[7] P. Thoft-Christensen, Corrosion and Cracking of Reinforced Concrete, Life-Cycle Perform. Deteriorating Struct. (2008) 26–36.
[8] Y. Bo, Y. LuFeng, W. Ming, L. Bing, Practical model for predicting corrosion rate of steel reinforcement in concrete structures, Constr. Build. Mater. 54 (2014) 385–401.
[9] H.-S. Lee, T. Kage, T. Noguchi, F. Tomosawa, An experimental study on the retrofitting effects of reinforced concrete columns damaged by rebar corrosion strengthened with carbon fiber sheets, Cem. Concr. Res. 33 (2003) 563–570.

[10] X. Wang, Research of Seismic Performance and Hysteretic Mode of Corroded Reinforced Concrete Members Master, Xi'an University of Architecture and Technology, 2003.
[11] Y. Ma, Y. Che, J. Gong, Behavior of corrosion damaged circular reinforced concrete columns under cyclic loading, Constr. Build. Mater. 29 (2012) 548–556.
[12] C. Goksu, Seismic Behavior of RC Columns With Corroded Plain and Deformed Reinforcing Bars Phd, Istanbul Technical University, Turkey, 2012.
[13] A. Meda, S. Mostosi, Z. Rinaldi, P. Riva, Experimental evaluation of the corrosion influence on the cyclic behaviour of RC columns, Eng. Struct. 76 (2014) 112–123.
[14] DIANA, Finite Element Analysis, in: 9.4.4, editor. Netherlands 9.4.4.
[15] Y.-C. Ou, N.D. Nguyen, Plastic hinge length of corroded reinforced concrete beams, Struct. J. (2014) 111.
[16] A.N. Kallias, Rafiq M. Imran, Finite element investigation of the structural response of corroded RC beams, Eng. Struct. 32 (2010) 2984–2994.
[17] K.Z. Hanjari, P. Kettil, K. Lundgren, Analysis of mechanical behavior of corroded reinforced concrete structures, ACI Struct. J. 108 (2011) 532–541.
[18] Design of concrete structures: CEB-FIP Model-Code 1990, London, UK, 1990.
[19] D. Coronelli, P. Gambarova, Structural assessment of corroded reinforced concrete beams: modeling guidelines, J. Struct. Eng. 130 (2004) 1214–1224.
[20] M. Cape, Residual service-life assessment of existing R/C structures (MS thesis) , Chalmers Univ. of Technology, Goteborg (Sweden) and Milan Univ. of Technology (Italy), Erasmus Program, 1999.
[21] F.J. Molina, C. Alonso, C. Andrade, Cover cracking as a function of rebar corrosion: part 2-numerical model, Mater. Constr. 26 (1993) 532–548.
[22] D.-E. Choe, P. Gardoni, D. Rosowsky, T. Haukaas, Probabilistic capacity models and seismic fragility estimates for RC columns subject to corrosion, Reliab. Eng. Syst. Saf. 93 (2008) 383–393.
[23] A. Sarja, E. Vesikari, Durability Design of Concrete Structures, 1996. RILEM Report Series 14.
[24] G. Monti, C. Nuti, Nonlinear cyclic behavior of reinforcing bars including buckling, J. Struct. Eng. New York, NY 118 (1992) 3268–3284.
[25] J.B. Mander, M.J.N. Priestley, R. Park, Theoretical stress-strain model for confined concrete, J. Struct. Eng. New York, NY 114 (1988) 1804–1826.
[26] K. Stanish, R.D. Hooton, S.J. Pantazopoulou, Corrosion effects on bond strength in reinforced concrete, ACI Struct. J. 96 (1999) 915–921.
[27] L. Chung, S.-H. Cho, J.-H.J. Kim, S.-T. Yi, Correction factor suggestion for ACI development length provisions based on flexural testing of RC slabs with various levels of corroded reinforcing bars, Eng. Struct. 26 (2004) 1013–1026.
[28] K. Bhargava, A. Ghosh, Y. Mori, S. Ramanujam, Suggested empirical models for corrosion-induced bond degradation in reinforced concrete, J. Struct. Eng. 134 (2008) 221–230.
[29] T.E. Maaddawy, K. Soudki, T. Topper, Analytical model to predict nonlinear flexural behavior of corroded reinforced concrete beams, ACI Struct. J. 102 (2005) 550–559.
[30] M.P. Berry, M.O. Eberhard, Performance modeling strategies for modern reinforced concrete bridge columns, Pacific Earthquake Engineering Research Center, University of California, Berkeley, 2007.
[31] M.D. Lepech, A. Rao, A. Kiremidjian, A. Michel, H. Stang, M. Geiker, Multi-physical and multi-scale deterioration modelling of reinforced concrete part II: Coupling corrosion and damage at the structural scale, in: Concrete – Innovation and Design, fib Symposium, Copenhagen May 18-20, 2015.
[32] ACI 318-14 A, Building code requirements for structural concrete (ACI 318-14) and commentary, American Concrete Institute, Farmington Hills, Mich, 2014.
[33] B. Li, R. Park, Confining reinforcement for high-strength concrete columns, ACI Struct. J. 101 (2004) 314–324.
[34] ASCE 41-06 A, Seismic rehabilitation of existing buildings, American Society of Civil Engineers, Reston, VA, 2007. ASCE standard: ASCE/SEI 41-06.
[35] M. Saatcioglu, S. Razvi, Strength and ductility of confined concrete, J. Struct. Eng. 118 (1992) 1590–1607.
[36] S. Sheikh, S.M. Uzumeri, Analytical model for concrete confinement in tied columns, J. Struct. Div. 108 (1982) 2703–2722.
[37] B. Oguzhan, A.S. Shamim, High-strength concrete columns under simulated earthquake loading, Struct. J. 94 (1997).
[38] L. Frederic, P. Patrick, Behavior of high-strength concrete columns under cyclic flexure and constant axial load, Struct. J. 97 (2000).
[39] I. Brachmann, J. Browning, A.B. Matamoros, Drift Capacity Approaches of Rectangular Slender Reinforced Concrete Columns Under Cyclic Loading, University of Kansas Center for Research, INC, Lawrence, Kansas, 2002. SM Report No. 68.
[40] C. Thanh Ngoc Tran, B. Li, Ultimate displacement of reinforced concrete columns with light transverse reinforcement, J. Earthquake Eng. 17 (2013) 282–300.